The Astrophysical Journal Letters, 937:L7 (11pp), 2022 September 20 https://doi.org/10.3847/2041-8213/ac8e68

Dynamical Origin for the Collinder 132–Gulliver 21 Stream: A Mixture of Three Comoving Populations with an Age Difference of 250 Myr

Xiaoying Pang[1,2], Yuqian Li[1], Shih-Yun Tang[3,4], Long Wang[5,6], Yanshu Wang[1], Zhao-Yu Li[7,11], Danchen Wang[1], M. B. N. Kouwenhoven[1], and Mario Pasquato[8,9,10]

[1] Department of Physics, Xi'an Jiaotong-Liverpool University, 111 Renai Road, Dushu Lake Science and Education Innovation District, Suzhou 215123, Jiangsu Province, People's Republic of China; Xiaoying.Pang@xjtlu.edu.cn
[2] Shanghai Key Laboratory for Astrophysics, Shanghai Normal University, 100 Guilin Road, Shanghai 200234, People's Republic of China
[3] Lowell Observatory, 1400 W. Mars Hill Road, Flagstaff, AZ 86001, USA
[4] Department of Astronomy and Planetary Science, Northern Arizona University, Flagstaff, AZ 86011, USA
[5] School of Physics and Astronomy, Sun Yat-sen University, Daxue Road, Zhuhai, 519082, People's Republic of China
[6] CSST Science Center for the Guangdong-Hong Kong-Macau Greater Bay Area, Zhuhai, 519082, People's Republic of China
[7] Department of Astronomy, School of Physics and Astronomy, Shanghai Jiao Tong University, 800 Dongchuan Road, Shanghai 200240, People's Republic of China
[8] Département de Physique, Université de Montréal, Montreal, Quebec H3T 1J4, Canada
[9] Physics and Astronomy Department Galileo Galilei, University of Padova, Vicolo dell'Osservatorio 3, I–35122, Padova, Italy
[10] Mila - Quebec Artificial Intelligence Institute, Montreal, Quebec, Canada
[11] Key Laboratory for Particle Astrophysics and Cosmology (MOE)/Shanghai Key Laboratory for Particle Physics and Cosmology, Shanghai 200240, People's Republic of China

Received 2022 July 22; revised 2022 August 26; accepted 2022 August 30; published 2022 September 20

Abstract

We use Gaia DR3 data to study the Collinder 132–Gulliver 21 region via the machine-learning algorithm StarGO and find eight subgroups of stars (ASCC 32, Collinder 132 gp 1–6, Gulliver 21) located in close proximity. Three comoving populations were identified among these eight subgroups: (i) a coeval 25 Myr old moving group (Collinder 132), (ii) an intermediate-age (50–100 Myr) group, and (iii) the 275 Myr old dissolving cluster Gulliver 21. These three populations form parallel diagonal stripe-shape overdensities in the *U*–*V* distribution, which differ from open clusters and stellar groups in the solar neighborhood. We name this kinematic structure the Collinder 132–Gulliver 21 stream, as it extends over 270 pc in the 3D space. The oldest population, Gulliver 21, is spatially surrounded by the Collinder 132 moving group and the intermediate-age group. Stars in the Collinder 132–Gulliver 21 stream have an age difference up to 250 Myr. Metallicity information shows a variation of 0.3 dex between the youngest and oldest populations. The formation of the Collinder 132–Gulliver 21 stream involves both star formation and dynamical heating. The youngest population (Collinder 132 moving group) with homogeneous metallicity is probably formed through filamentary star formation. The intermediate-age and oldest populations were then scattered by the Galactic bar or spiral structure resonance to intercept Collinder 132's orbit. Without mutual interaction between each population, the three populations are flying by each other currently and will become three distinct groups again in ∼50 Myr.

Unified Astronomy Thesaurus concepts: Star clusters (1567); Open star clusters (1160); Stellar kinematics (1608); Moving clusters (1076)

Supporting material: machine-readable table

1. Introduction

Moving groups are congregations of comoving stars that typically extend from a few hundred parsecs to a few kiloparsecs in space. Most moving groups known in the solar neighborhood (e.g., Eggen 1996; Skuljan et al. 1999) are named after open clusters in the region, such as the Hyades, the Pleiades, Coma Berenices, and IC 2391 moving groups. Some of these moving groups are coeval and are thought to have originated from dissolving open clusters (e.g., Miret-Roig et al. 2020; Gagné et al. 2021; Lee et al. 2022; Messina et al. 2022). Other young coeval moving groups, on the other hand, were thought to form simultaneously in the same giant molecular cloud (GMC; Kounkel & Covey 2019).

Most of the moving groups, however, are not associated with their eponymous open clusters and appear to host populations of different ages and inhomogeneous metallicities, such as the Hercules, Arcturus, and HR 1614 moving groups (Eggen 1996; Bensby et al. 2007, 2014; Kushniruk et al. 2020). An age spread of several billion years found in the aforementioned moving groups (Kushniruk et al. 2020) cannot be simply explained by inhomogeneous star formation.

Stars in moving groups share similar kinematics like stars in stellar clusters; however, moving groups stand out in the velocity distribution as elongated substructures (e.g., horizontal or diagonal branches on the *U*–*V* velocity plane; Antoja et al. 2008; Zhao et al. 2009; Kushniruk et al. 2017; Gaia Collaboration et al. 2018b; Kushniruk et al. 2020) opposed to a concentrated distribution of stellar clusters. A horizontal arch shown on the *U*–*V* velocity space can indicate conservation of vertical angular momentum, which might support a dynamical origin of the moving group (Kushniruk et al. 2020).

Various theories have sprung up to provide solutions to the formation mechanism of non-coeval moving groups. De Simone et al. (2004) proposed that stochastic transient spiral waves can heat up the disk and generate moving groups, which

mainly excite the stellar horizontal velocity components along the Galactic disk. Other formation theories are mostly related to resonances. The Sirius and Hyades moving groups have been suggested to be induced by the inner Lindblad resonance of the spiral structures. On the other hand, the Hercules moving group is associated with the Galactic bar's outer Lindblad resonance (Dehnen 2000; Bovy & Hogg 2010). The Coma Berenices and Pleiades moving groups may be related to the spiral corotation resonance (Barros et al. 2020). Another alternative is an external perturbation triggered by a minor merger event (Minchev et al. 2010; Antoja et al. 2012; Barros et al. 2020), which produces vertical phase mixing (Antoja et al. 2018; Li & Shen 2020; Li et al. 2021) and excites the stars to move perpendicular to the Galactic disk. When stars in a moving group are formed at different locations and/or at different times, they will have different ages and come with different metallicities.

The young moving group studied in this paper, Collinder 132, was originally known as an open cluster by Collinder (1931) and later suggested to host two populations by Clariá (1977) and Eggen (1983). Kounkel & Covey (2019) later used Gaia Data Release 2 (DR2) data and suggested Collinder 132 to be a coeval moving group extending 197 pc with an age of 25 Myr. Meanwhile, in the same sky region as Collinder 132, a cluster, Gulliver 21, with an age 10 times older than Collinder 132 was found (275 Myr; Cantat-Gaudin et al. 2018; Pang et al. 2022). As no investigation has been made for Collinder 132 and Gulliver 21 yet, whether or not this older cluster, Gulliver 21, is associated with the Collinder 132 moving group is still unknown. If an association exists, the origin of this moving group can be further constrained by the dynamical formation mechanism.

The latest Gaia Data Release, Data Release 3 (DR3; Gaia Collaboration et al. 2022), published radial velocity (RV) measurements for 34 million stars, a data set four times larger than the DR2 (Gaia Collaboration et al. 2018a). We aim to study the possible connection between the Collinder 132 moving group and the cluster Gulliver 21 using Gaia DR3 kinematic data. A kinematic relationship between the 275 Myr old cluster Gulliver 21 and the 25 Myr old moving group Collinder 132 will provide strong observational constraints to the formation and evolution of moving groups.

This paper is organized as follows. In Section 2.1 we discuss the quality and limitations of the Gaia DR 3 and EDR 3 data. We then present the algorithm StarGO, which is used to determine members in groups, in Section 2.2. In Section 3, we identify three moving groups in kinematic space and name the kinematic structures made of these three populations the Collinder 132–Gulliver 21 stream. The spatial characteristics and dynamical state of the stream are presented in Section 4. The origin of the Collinder 132–Gulliver 21 stream is investigated in Section 5, in which we discuss the possibility of different dynamical formation mechanisms. Finally, we provide a brief summary of our findings in Section 6.

2. Data and Membership Identification

2.1. Gaia EDR3 and DR3 Data

The Gaia DR 3 (Gaia Collaboration et al. 2022) became publicly available 1.5 yr after the release of EDR 3 (released on 2020 December 3; Gaia Collaboration et al. 2021). Parts of the data in DR3 are inherited from EDR3, such as the full astrometric solution (e.g., sky positions, parallaxes, and proper motions (PMs)) and G_{BP} and G_{RP} magnitudes. Correction to the G-band photometry has been made in DR3 (Riello et al. 2021), which mainly affects sources fainter than $G = 13$ mag. In the sky region of Collinder 132 and Gulliver 21, the mean difference in G-band magnitude between EDR3 and DR3 is approximately 0.003 mag and reaches a maximum value of 0.025 mag.

The number of targets with RV measurement from the Radial Velocity Spectrometer (RVS, with a median resolving power $R \sim 11{,}500$) increased from ~7 million in DR2 to ~34 million in DR3. The longer observation baseline, 34 months of the nominal mission, also helped push the processing limitation from $G_{\rm RVS} = 12$ mag in Gaia DR2 to $G_{\rm RVS} = 14$ mag in DR3. The median precision of the RV is 1.3 km s^{-1} at $G_{\rm RVS} = 12$ mag and 6.4 km s^{-1} at $G_{\rm RVS} = 14$ mag (Katz et al. 2022).

With the release of Gaia DR3, astrophysical parameters have become available; these are derived from RVS spectra and/or from low-resolution ($R \sim 40$) BP/RP prism spectra (Creevey et al. 2022). Astrophysical parameters determined from forward-modeling the BP/RP spectra (GSP-Phot, 470 million; Andrae et al. 2022) outnumber those obtained from combined RVS spectra of single stars (GSP-Spec, 6 million; Recio-Blanco et al. 2022), which come with more precise and detailed information on individual chemical abundances.

2.2. Member Determination

The member identification process for the stellar groups discussed in this paper is carried out as described in Tang et al. (2019) and Pang et al. (2020, 2021a, 2021b, 2022). In short, the membership identification process is performed in a sequence of three steps. First, we make two spherical cuts in the 3D Cartesian coordinates space with a radius of 150 pc from the center of Collinder 132 obtained from Cantat-Gaudin et al. (2020) and a radius of 150 pc from the center of ASCC 32 taken from Liu & Pang (2019), in order to cover the elongated morphology of the Collinder 132 moving group. Second, we perform a further PM cut on the target region based on a 2D density map (e.g., Figure 1 in Pang et al. 2021a). These circular PM cuts are performed to include as many potential members as possible and to reduce the number of field stars that can weaken the clustering signature in the member identification process. Third, we use the unsupervised machine-learning method StarGO (Yuan et al. 2018)[12] to identify the grouping using a 5D data set, i.e., X, Y, Z, $\mu_\alpha \cos\delta$, and μ_δ. The StarGO software is based on the Self-Organizing Map (SOM) algorithm, which can help map high-dimensional data onto a 2D neural network (Figure A1) and search for grouping. We provide more details on member selection with StarGO in Appendix A.

StarGO has proven to be successful in the identification of stellar streams and star cluster membership (Tang et al. 2019; Zhang et al. 2019; Yuan et al. 2020a, 2020b; Pang et al. 2020, 2021a, 2021b, 2022). The algorithm StarGO not only is efficient in mapping the detailed structure of each stellar cluster or group but also is able to identify hierarchical structures in stellar groups. Pang et al. (2021b) use this top-down identification approach to disentangle five second-level substructures in the Vela OB2 region, and Pang et al. (2022)

[12] https://github.com/zyuan-astro/StarGO-OC

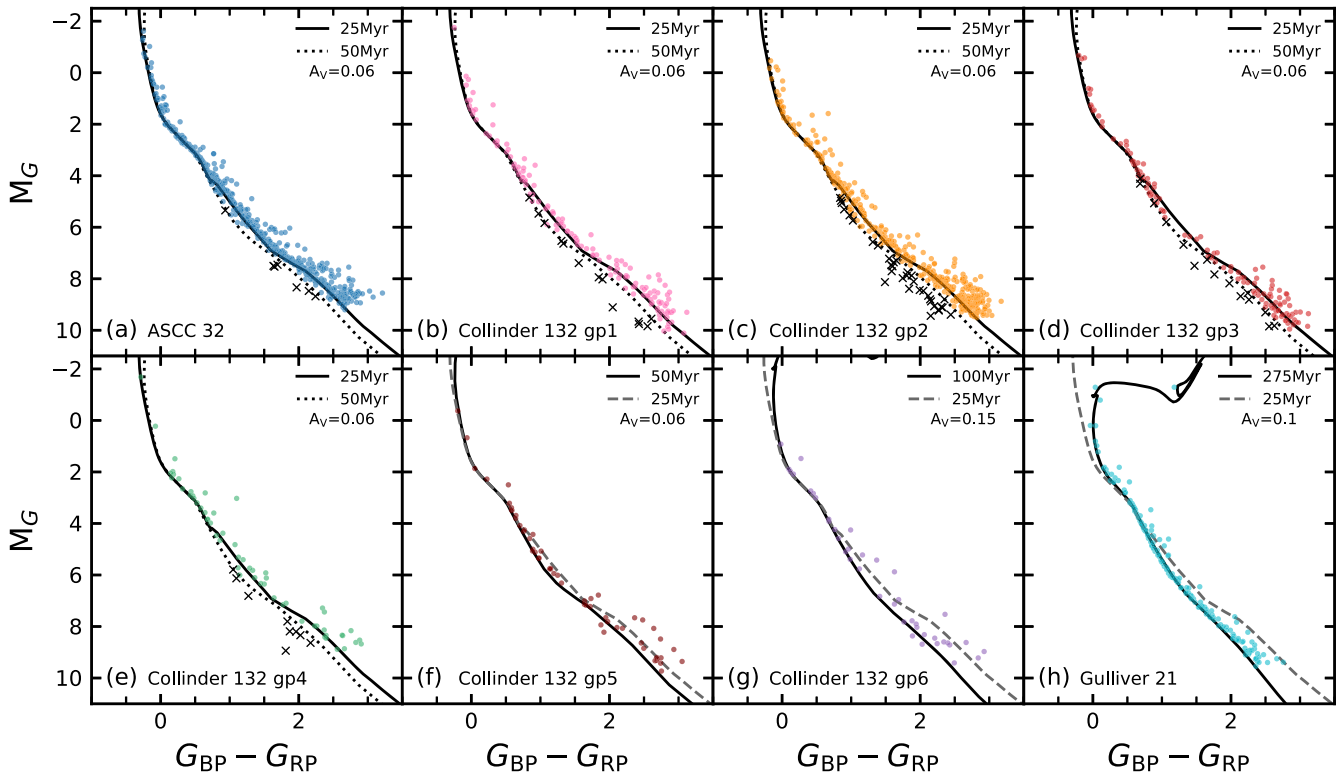

Figure 1. Absolute magnitude CMDs (with M_G adopting Gaia DR 3 parallaxes) for member stars obtained from Gaia DR 3. The colored circles in each panel represent the corresponding member candidates in each subgroup. Black crosses are field stars that are excluded from further investigation (see Section 3.1). The PARSEC isochrones of the best-fitted age are indicated with the black solid curves, with solar metallicity and estimated A_V. The black dotted curve is an isochrone of 50 Myr, with solar metallicity and $A_V = 0.06$. The gray dashed curves in panels (f)–(h) are 25 Myr isochrones for comparison.

identified 10 new hierarchical groups in four young regions using StarGO.

In total, we identify eight subgroups of stars in the Collinder 132–Gulliver 21 region. Among these, Collinder 132 gp 1 (pink patch in Figure A1(b)) and Collinder 132 gp 2 (orange patch) are second-level structures on the SOM. Collinder 132 gp 1 (corresponding to the stellar group Collinder 132), Gulliver 21 (cyan patch), and ASCC 32 (blue patch) are known open clusters or stellar groups that were reported in previous catalogs (Liu & Pang 2019; Cantat-Gaudin et al. 2020; He et al. 2022). The remaining five groups are new and are labeled as Collinder 132 gp 2–6.

3. Comoving Populations

3.1. Age and Metallicity Difference

We construct color–magnitude diagrams (CMDs) for the member candidates of the eight subgroups of stars in the Collinder 132–Gulliver 21 regions. We first fit the PARSEC isochrone (version 1.2S; Bressan et al. 2012; Chen et al. 2015) to each subgroup by eye to estimate their age and reddening. All subgroups are assumed to have solar abundance. We observe three major populations of different ages among the eight subgroups in the target region (Figure 1). The first population is the Collinder 132 moving group, which contains five subgroups with an age of 25 Myr: ASCC 32 and Collinder 132 gp 1–4. The second population is an intermediate-age group (50–100 Myr): Collinder 132 gp 5–6. The third population is the oldest generation with an age of 275 Myr: Gulliver 21. The mass of each member star is then estimated from the best-fit isochrone using the kD tree method (McMillan et al. 2007) by finding the nearest point on the isochrone.

In Figures 1(a)–(e), a handful of candidate stars are located below the main-sequence locus with age older than 50 Myr (black dotted curve). Although these stars are located in the same sky region as the 25 Myr old Collinder 132 moving group, we did not find any distinctive difference between these stars and the field stars nearby. Similar to the approach taken in Section 3.1 in Pang et al. (2021b), we consider stars bluer than the 50 Myr old isochrone and fainter than $M_G > 4$ mag as field-star contaminants (black crosses in panels (a)–(e) in Figure 1) and therefore exclude them from further analysis.

A total of 1496 members of the eight stellar subgroups in the Collinder 132–Gulliver 21 region remain after CMD cleaning (Figure 1). Basic parameters of these eight subgroups are presented in Table 1. We provide a detailed member list of all subgroups in Table B1. Our list of members is in a good agreement with two moving groups studied in Kounkel & Covey (2019): 332 stars in ASCC 32 and Collinder 132 gp 1–4 (black plus signs in Figure 2(a)) belong to the Collinder 132 moving group in Kounkel & Covey (2019), and 43 stars in Collinder 132 gp 5–6 (gray plus signs in Figure 2(a)) match with the members of the Theia 86 moving group found by Kounkel & Covey (2019). In our study, not only do we double the number of member stars in the Collinder 132 moving group compared to Kounkel & Covey (2019), but we are also the first in identifying five hierarchical subgroups in the Collinder 132 moving group.

The distribution of metallicities, [M/H], of 1351 identified members obtained from BP/RP spectra of Gaia DR 3 indicates an abundance variation among the three populations. Five

Table 1
General Properties of Eight Subgroups in the Collinder 132–Gulliver 21 Stream

Cluster	R.A. (deg)	Decl. (deg)	Dist. (pc)	X_c (pc)	Y_c (pc)	Z_c (pc)	RV (km s^{-1})	$\mu_\alpha \cos\delta$ (mas yr^{-1})	μ_δ (mas yr^{-1})	Age (Myr)	$M_{\rm cl}$ ($M_\odot$)	r_h (pc)	r_t (pc)	N
(1)	(2)	(3)	(4)	(5)	(6)	(7)	(8)	(9)	(10)	(11)	(12)	(13)	(14)	(15)
ASCC 32	105.730278	−26.449193	795.2	−416.7	−664.6	−130.3	32.4	−3.228	3.475	25	577.6	17.4	11.7	519
Collinder 132 gp 1	108.870127	−31.069356	655.1	−287.8	−579.4	−103.2	21.7	−4.227	3.756	25	144.4	28.7	7.3	142
Collinder 132 gp 2	107.042730	−25.625351	689.6	−364.9	−576.7	−98.7	28.0	−3.916	3.617	25	362.7	28.2	10.0	385
Collinder 132 gp 3	107.437642	−25.401309	602.2	−316.9	−506.1	−78.4	26.1	−4.949	3.749	25	121.1	15.2	6.9	123
Collinder 132 gp 4	107.181518	−30.328868	789.1	−365.5	−686.4	−133.9	30.3	−3.417	3.407	25	68.4	14.6	5.7	58
Collinder 132 gp 5	107.638309	−27.792975	599.4	−297.3	−513.2	−87.3	37.9	−3.231	6.356	50	53.1	9.0	5.3	56
Collinder 132 gp 6	111.643982	−30.322059	615.6	−270.2	−548.8	−69.8	34.1	−4.354	6.113	100	39.5	15.5	4.8	40
Gulliver 21	106.972407	−25.450964	648.7	−345.0	−542.1	−89.4	39.8	−1.907	4.214	275	176.5	9.3	7.9	173

Note. Columns (2)–(10) list the median values of the subgroup member properties. R.A. and Decl. are the right ascension and declination. Dist. is the corrected distance. X_c, Y_c, and Z_c are the positions of each subgroup in heliocentric Cartesian coordinates after distance correction. RV is the radial velocity. Parameters $\mu_\alpha \cos\delta$ and μ_δ are the components of the PM. The age of each subgroup is derived from PARSEC isochrone fitting (Figure 1). $M_{\rm cl}$ is the total mass of each subgroup. Parameters r_h and r_t are the half-mass radius and the tidal radius of each subgroup, respectively. The tidal radius is computed using Equation (12) in Pinfield et al. (1998). N is the total number of members in each subgroup.

Table B1
Columns for the Table of Individual Members of the Eight Subgroups in Collinder 132–Gulliver 21 Stream

Column	Unit	Description
Cluster Name	⋯	Name of the target cluster
Gaia ID	⋯	Object ID in Gaia DR 3
ra	deg	R.A. at J2016.0 from Gaia DR 3
er_RA	mas	Positional uncertainty in R.A. at J2016.0
dec	deg	Decl. at J2016.0 from Gaia DR 3
er_DEC	mas	Positional uncertainty in decl. at J2016.0
parallax	mas	Parallax from Gaia DR 3
er_parallax	mas	Uncertainty in the parallax
pmra	mas yr^{-1}	Proper motion with robust fit in $\alpha \cos\delta$ from Gaia DR 3
er_pmra	mas yr^{-1}	Error of the proper motion with robust fit in $\alpha \cos\delta$
pmdec	mas yr^{-1}	Proper motion with robust fit in δ from Gaia DR 3
er_pmdec	mas yr^{-1}	Error of the proper motion with robust fit in δ
Gmag	mag	Magnitude in *G* band from Gaia DR 3
BP	mag	Magnitude in *BP* band from Gaia DR 3
RP	mag	Magnitude in *RP* band from Gaia DR 3
Gaia_radial_velocity	km s^{-1}	Radial velocity from Gaia DR 3
er_Gaia_radial_velocity	km s^{-1}	Error of radial velocity from Gaia DR 3
Mass	$M_\odot$	Stellar mass obtained in this study
X_obs	pc	Heliocentric Cartesian *X* coordinate computed via direct inverting Gaia DR 3 parallax ϖ
Y_obs	pc	Heliocentric Cartesian *Y* coordinate computed via direct inverting Gaia DR 3 parallax ϖ
Z_obs	pc	Heliocentric Cartesian *Z* coordinate computed via direct inverting Gaia DR 3 parallax ϖ
X_cor	pc	Heliocentric Cartesian *X* coordinate after distance correction in this study
Y_cor	pc	Heliocentric Cartesian *Y* coordinate after distance correction in this study
Z_cor	pc	Heliocentric Cartesian *Z* coordinate after distance correction in this study
Dist_cor	pc	Corrected distance of individual member

Note.

(This table is available in its entirety in machine-readable form.)

subgroups in the Collinder 132 moving group have an almost homogeneous metallicity with a mean $[M/H] \sim -0.32$. The oldest population, Gulliver 21, has $[M/H] \sim -0.09$, different from the youngest generation by 0.3. The intermediate-age group has $[M/H] \sim -0.24$. Although the absolute value of metallicity from GSP-Phot has zero-point offset issues (Andrae et al. 2022), the relative values of [M/H] among three populations can still provide some hint in abundance discrepancy. Based on the 61 members with [M/H] measurements from the RVS in Gaia DR 3, the [M/H] difference between Gulliver 21 and the Collinder 132 moving group ranges from 0.3 to 0.6 (after calibration following Recio-Blanco et al. 2022). The metallicities obtained from the *BP*/*RP* spectra are somewhat uncertain because of the low spectral resolution, and the ones obtained from the RVS are affected by low number statistics. Therefore, follow-up spectroscopy studies are needed to confirm the abundance discrepancy between Collinder 132 and Gulliver 21.

3.2. Velocity Distribution Features

Identification of moving groups is normally carried out by searching for kinematic substructures in velocity space. RVs with a signal-to-noise ratio (S/N) > 20 are selected to construct the velocity distribution to avoid bias by uncertainty. We compute the RV dispersion of each group using the Markov Chain Monte Carlo (MCMC) method (Pang et al. 2021a), with a likelihood function for the RV distribution that is a combination of two Gaussian components: one for the cluster members and one for the field stars (Equations (1) and (8) in Cottaar et al. 2012). The resulting RV dispersion for these eight subgroups is in the range of ∼2.0–6.5 km s^{-1}.

We present the three populations (eight subgroups) in the Collinder 132–Gulliver 21 region in the *U*–*V* velocity plane (Heliocentric) in Figure 2(b). These three populations of stars all follow a tight correlation between *U* and *V* and form parallel diagonal stripes with identical slopes in the *U*–*V* plane. The pattern of diagonal stripes is robust since their full extension (>30 km s^{-1}) is much larger than observational errors (indicated in the lower left corner of Figure 2(b)) and the RV dispersions.

The Coma Berenices, Hyades, and Pleiades moving groups (plus signs in Figure 2(b); Antoja et al. 2008) surround the three populations of stars and the NGC 1901 and IC 2391 moving groups in a triangle pattern. Compared to the distribution of 85 open clusters and stellar groups from Pang et al. (2022; gray circles in Figure 2(a)), the kinematic structure of these three populations is similar to that of the 692 Myr old dissolving cluster Alessi 62 (cross No. 5 in Figure 2(b), in which stars are still comoving. Their *V* values extend to 30 km s^{-1}, larger than any of the other clusters or groups from Pang et al. (2022), indicating their comoving state. In the *U*–*V* plane, the moving groups (plus signs) named after open clusters (Pleiades, Coma Berenices, NGC 1901, and IC 2391) appear to closely relate to the median velocities of the eponymous open clusters taken from Pang et al. (2022; crosses in Figure 2(b)), with a small offset due to different survey data and unequal member numbers between moving group and open clusters.

The distinct substructures emerging from these three populations in the *U*–*V* plane indicate that their kinematics resemble moving groups, which are assumed to be unbound. There are three individual comoving populations: (i) a 25 Myr old Collinder 132 moving group, (ii) an intermediate-age group (50–100 Myr), and (iii) the oldest group Gulliver 21 (275 Myr).

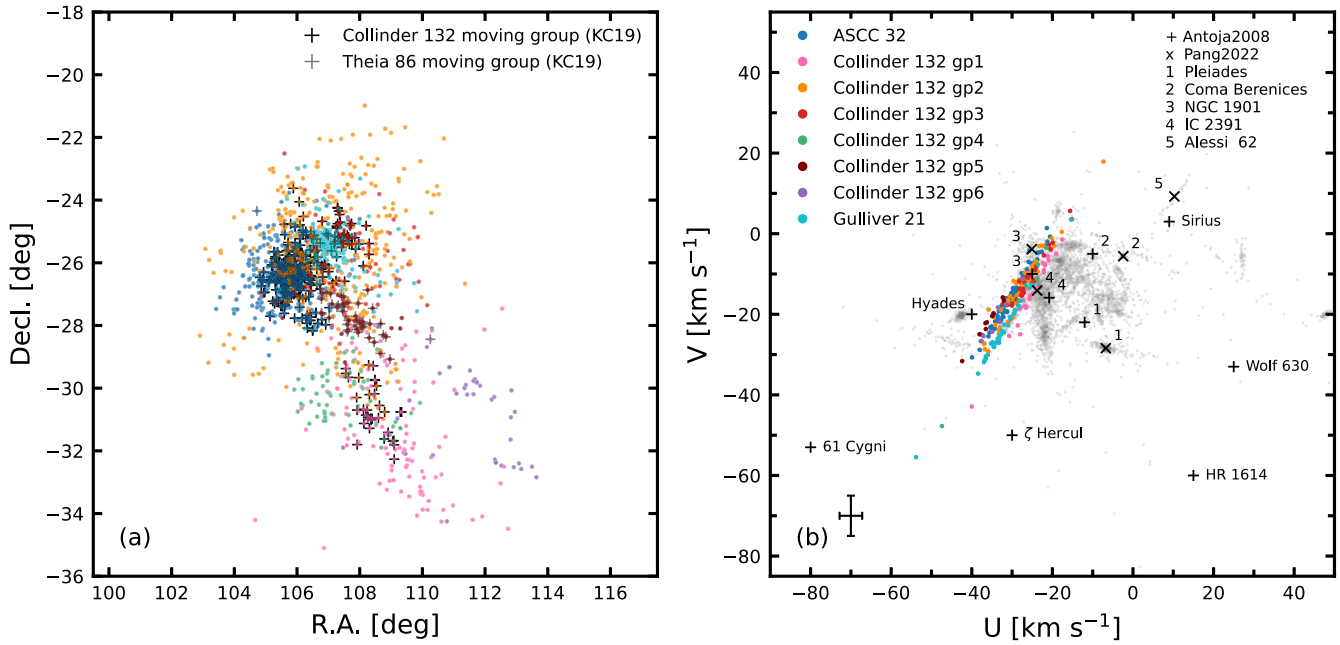

Figure 2. (a) Projected spatial distribution of member candidates. Cross-matched members with the Collinder 132 moving group in Kounkel & Covey (2019; KC19) are indicated by the black plus signs. Matched stars with the Theia 86 moving group in KC19 are shown as gray plus signs. (b) The U–V velocity distribution for eight subgroups in the Collinder 132–Gulliver 21 region obtained from this study. Members of these eight subgroups are shown as colored circles. The mean errors of U and V are indicated in the lower left corner. The gray circles in the background are 85 clusters and groups from Pang et al. (2022) for comparison. The S/Ns of RVs constructing velocities U and V are restricted to be greater than 20. The black cross indicates the median position of the open cluster Alessi 62 taken from Pang et al. (2022). Alessi 62 is a dissolving cluster with an age of 692 Myr, which forms a diagonal stripe structure.

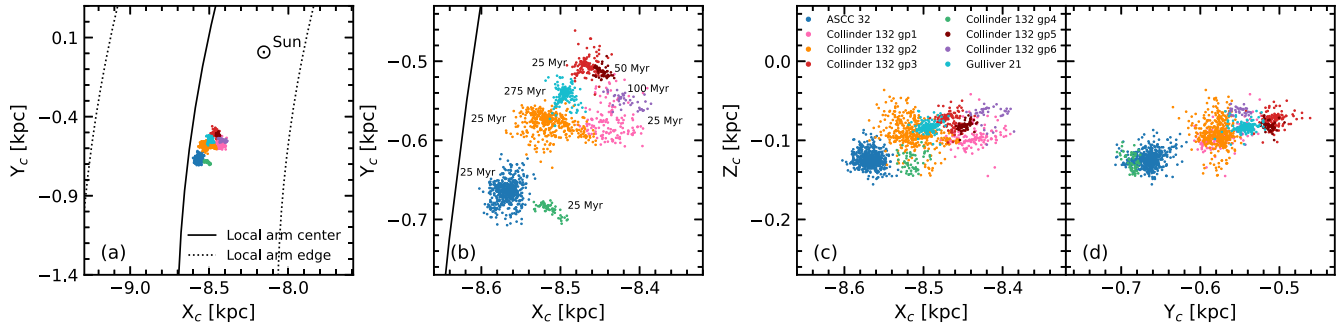

Figure 3. 3D morphology of the Collinder 132–Gulliver 21 stream in Galactocentric Cartesian coordinates after distance correction via a Bayesian approach (Pang et al. 2021a). The black solid curve represents the Local Arm center, and the Local Arm edge is denoted as the black dotted curve. The position of the Sun is taken at $(X, Y, Z) = (-8150, 0, 5.5)$ pc (Reid et al. 2019). The age of each subgroup is indicated in panel (b) to show that the oldest population is surrounded by young populations.

Stars in each population are comoving together. We call the kinematic structures generated by these three comoving populations the Collinder 132–Gulliver 21 stream.

4. Characteristics of Collinder 132–Gulliver 21 Stream

4.1. Spatial Distribution

The 3D spatial distribution shown in Figure 3(a) indicates that the Collinder 132–Gulliver 21 stream is located close to the Local Arm center (Reid et al. 2019), where the stellar density is the highest. The entire Collinder 132–Gulliver 21 stream has a spatial extent of 270 pc (Figures 3(b)–(d)) after distance correction, which followed the Bayesian method described in Carrera et al. (2019) and Pang et al. (2020, 2021a). The Collinder 132 moving group and the intermediate-age groups encircle the oldest population, Gulliver 21 (Figure 3(b)). Subgroups in the Collinder 132 moving group (ASCC 32, Collinder 132 gp 1–4) exhibit a filamentary morphology, similar to the filamentary-type stellar groups in Pang et al. (2022). This elongated filamentary shape of the Collinder 132 moving group resembles the stellar relics of star formation (Jerabkova et al. 2019; Beccari et al. 2020). The abundance homogeneity (Section 3.1) in these five subgroups suggests that they all originate from a common GMC.

To further investigate the star formation process in this region, we overlay the Collinder 132–Gulliver 21 stream on the Improved Reprocessing of the IRAS Survey (IRIS; Miville-Deschênes & Lagache 2005) image in Figure 4. The 60 μm band image shows the gas structures in this region. A bubble-like structure is apparent in the background. This bubble has not been cataloged in existing bubble catalogs (Churchwell et al. 2006, 2007; Simpson et al. 2012; Bania et al. 2012; Hou & Gao 2014; Yan et al. 2016) or the molecular cloud catalog (Chen et al. 2020) because it has a decl. beyond the observation limit of these studies. Dame et al. (2001) reported very weak CO emission from this region, indicating low gas density. The

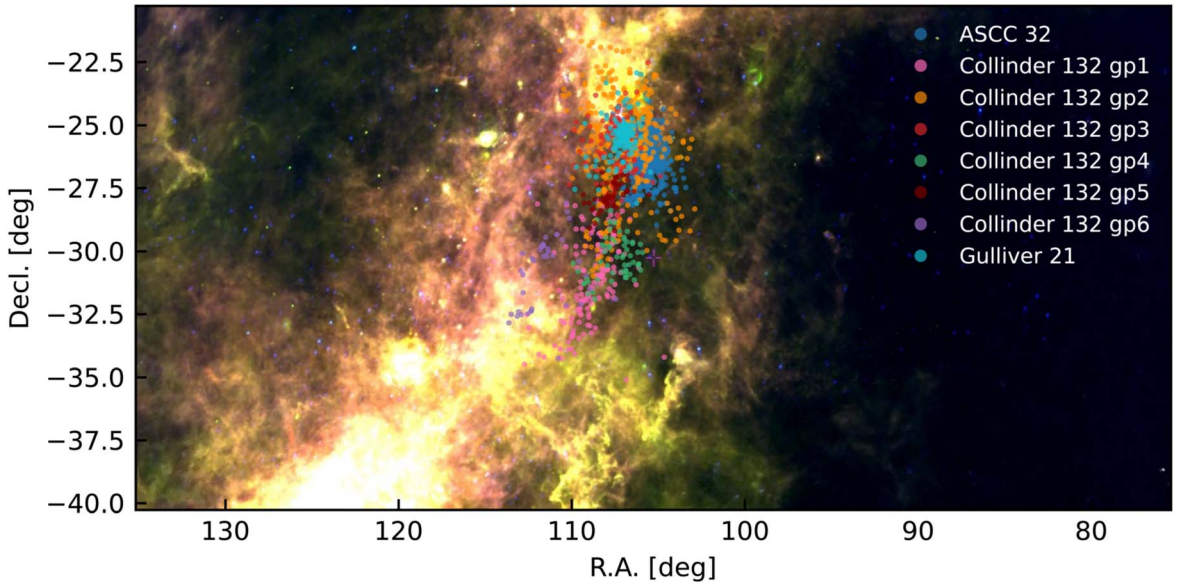

Figure 4. IRAS-IRIS infrared image of the 60 μm band (Miville-Deschênes & Lagache 2005). Members of the eight subgroups in the Collinder 132–Gulliver 21 stream are displayed as colored circles. The background bubble structure is apparent.

observed bubble in Figure 4 should be located at a distance >800 pc, based on the 3D extinction map, in which there is a sudden increase in the reddening at a distance beyond 800 pc (Green et al. 2019). Whether or not the bubble is adjacent to our target region is still unclear, as the members of ASCC 32 extend beyond 800 pc. The young Collinder 132 moving group may have originated from a recent large-scale filamentary star formation episode, from which remaining gas may still be present. Gaia DR 3 GSP-Phot extinctions in G, G_{BP}, and G_{RP} suggest an 0.1 mag higher reddening of the younger generations, compared to the oldest population, Gulliver 21. Further investigation is needed to confirm this difference.

4.2. Dynamical State

We adopt Equation (3) in Fleck et al. (2006) with $\eta = 9.75$ from Pang et al. (2013) to estimate the dynamical mass of each subgroup in the Collinder 132–Gulliver 21 stream using the 1D PM. These dynamical masses computed from Gaia DR 3 PMs for all subgroups are an order of magnitude larger than their corresponding photometric masses. In addition, the observed half-mass radii of these eight subgroups are all larger than their tidal radii (Table 1). Therefore, all three comoving populations are gravitationally unbound and dissolving, living up to the name "moving group." The youngest moving group, Collinder 132, probably experienced violent relaxation after a phase of significant gas expulsion (e.g., Baumgardt & Kroupa 2007; Pang et al. 2020), as supported by the presence of the bubble in the region (Figure 4).

5. Dynamical Origin of the Collinder 132–Gulliver 21 Stream

5.1. Flyby Scenario

To investigate the kinematical relation between each comoving population in the Collinder 132–Gulliver 21 stream, we compute the relative PMs and 3D velocities for all subgroups with Gulliver 21 median values as a reference. In Figure 5(a), arrows are color-coded based on their pointing directions that match the color wheel in the upper left corner. Therefore, arrows with similar colors share similar relative velocities. Two distinct velocity populations can be identified: (i) a magenta arrow population pointing to the east composed of mostly the young Collinder 132 moving subgroups; and (ii) a blue arrow population pointing to the northeast, with intermediate-age subgroups. While the Collinder 132 moving groups (magenta arrows) and the intermediate-age group (blue arrows) move in two unique directions with respect to Gulliver 21, members of Gulliver 21 show expansion patterns (thicker arrows). Similar signatures are observed in the distribution of relative 3D velocities (Figures 5(b) and (c)). The mean 3D velocity of each subgroup, relative to Gulliver 21, is represented with a large gray arrow (Figure 5(b)), which is mostly larger than the RV dispersion ($\sim$2.0−6.5 km s^{-1}) and the mean RV error. Gulliver 21 is passing through the Collinder 132 moving groups, while the intermediate-age group inclines to move toward Gulliver 21's orbit. Due to the weak gravitational forces between each subgroup, which are two orders of magnitude smaller than those of Galactic tidal forces, the trajectories of these three comoving populations are not affected by their mutual gravitational interactions.

To disentangle the unique dynamics of each population, we integrate the orbits of eight subgroups back and forward in time, using the observed median value of the 3D velocities and 3D positions of each member in all subgroups. The publicly available package `Galpy` (Bovy 2015) is used for the orbit integration. We adopt values of 8.15 kpc for the solar orbital distance and 247 km s^{-1} for the solar rotational velocity (Reid et al. 2019) and use the axisymmetric Galactic potential model `MWPotential2014`, which is adequate for integrating the orbits of open clusters (Wang & Jerabkova 2021; Pang et al. 2022; Boffin et al. 2022). Figures 6(a) and (b) show the orbits of the eight subgroups in the three comoving populations. The plus signs indicate the positions of subgroups at their time of birth. The triangles are present-day positions, and the filled circles are the predicted positions at 100 Myr in the future. All eight of these subgroups follow almost circular orbits, with eccentricities ranging from 0.02 to 0.07. The distance between

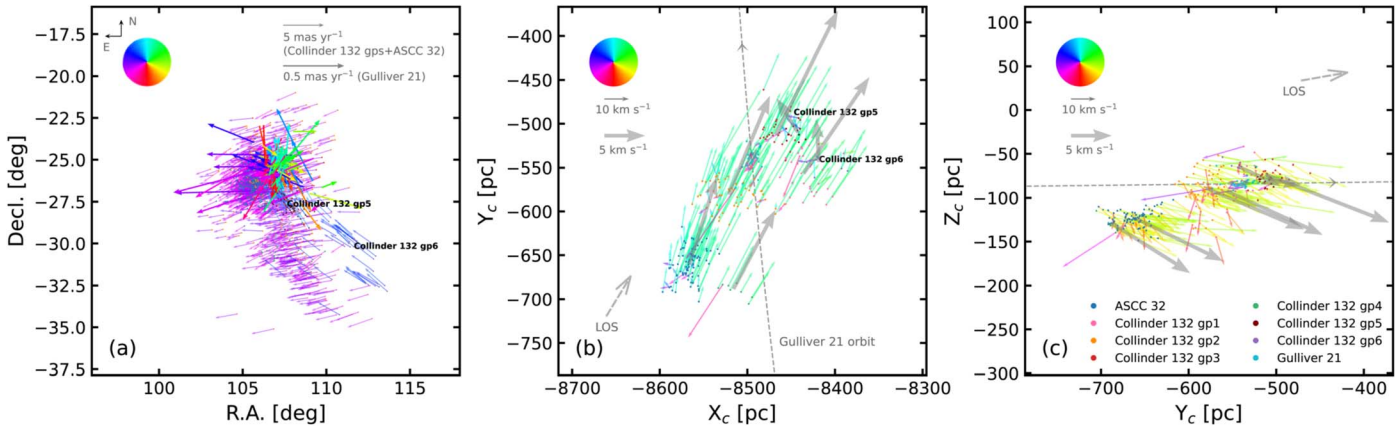

Figure 5. (a) The relative PMs of member candidates. All PM vectors are relative to the median PM of Gulliver 21. The vectors of Gulliver 21 members are thicker and are using different scaling than those for other groups (upper right corner). (b–c) The relative 3D velocity vectors for members, projected onto the *X*-*Y* and *Y*-*Z* planes. The median motion of Gulliver 21 is taken as the reference. We only show velocity vectors for stars with S/N > 20 in RV, of which the mean error is 5.8 km s^{-1}. The large thick gray arrows represent the mean velocity of each subgroup relative to that of Gulliver 21, whose scaling is indicated in the upper left corner (gray arrow). The gray dashed curve shows the orbit of Gulliver 21, and the orbital direction is indicated with an arrow. The dashed arrows in panels (b) and (c) indicate the direction of the line of sight (LOS). The colors of the vectors in these three panels indicate the directions of the vectors, consistent with the color wheel. The scaling of the vectors is shown in each panel.

the seven younger subgroups and Gulliver 21 reaches a minimum at the present time (Figure 6(c)) and will increase dramatically in the near future.

The observed Collinder 132–Gulliver 21 stream is a transitional product of orbital overlap of the three comoving populations. This temporary comoving status can only exist for a period of about 70 Myr, which is the estimated lifetime for the stream. This phase started approximately 20 Myr ago. In approximately 50 Myr from now, the Collinder 132 moving groups and the intermediate-age group will separate from Gulliver 21. The Collinder 132–Gulliver 21 stream will therefore disappear. Even when observational errors are considered in calculating the distance between moving groups (shaded areas in Figure 6(c) show the $\pm 1\sigma$ interval), subgroups in each comoving population will remain close to each other for at least 100 Myr (Figure 6(c)).

5.2. Resonance Scenario

Known classical moving groups form a horizontal branch/arch of constant V in the U–V space, implying conservation of angular momentum along the vertical direction, which is expected in the resonance scenario (Dehnen 2000; Bovy & Hogg 2010; Barros et al. 2020). However, the overdensities of the three comoving populations in the Collinder 132–Gulliver 21 stream show "parallelly tilted" features on the U–V velocity space. A similar feature has been observed in the moving group HR 1614 (Kushniruk et al. 2020), which is suggested to be induced by a combination mechanism of resonances and phase mixing.

The Galactic bar resonance (Dehnen 2000; Bovy & Hogg 2010), the resonant scattering by transient spiral structure (Sellwood & Binney 2002), and the stochastic spiral wave (De Simone et al. 2004) are all able to change the stellar kinematics in the Galactic plane. As the Collinder 132–Gulliver 21 stream is located at the center of the Local Arm (Figure 3(a)), excitation and heating events from resonance could be frequent. Gulliver 21 and the intermediate-age group might be affected by these mechanisms and may have been scattered to the position of the Collinder 132 moving group. Afterward, these three comoving populations began to fly by each other and form the Collinder 132–Gulliver 21 stream about 20 Myr ago. In approximately 50 Myr from now, their orbits will diverge again.

5.3. Phase-mixing Scenario

Phase mixing due to external perturbations (Antoja et al. 2018; Barros et al. 2020; Li & Shen 2020; Li 2021), such as the previous pericentric passage of the Sagittarius dwarf galaxy across the Milky Way disk, can also produce similar kinematic structures like moving groups in the velocity space (i.e., U–V) and affects the vertical motion of stars and stars' position in the Galactic disk. Evidence of the vertical perturbation is reflected as the snail shell shape in the $Z - V_Z$ distribution for stars across the Galactic disk. However, previous studies have suggested that the perturbation occurred ~500–700 Myr ago (Li & Shen 2020; Li 2021; Li & Widrow 2021), which is much earlier than the time at which the 25 Myr old Collinder 132 moving groups were formed. Therefore, vertical phase mixing has had little effect on the stellar motions in the Collinder 132–Gulliver 21 stream. It is thus unlikely the cause for the formation of the Collinder 132–Gulliver 21 stream. On the other hand, the horizontal phase mixing of the stars in the Galactic disk could have been stimulated by the previous vertical perturbation, affecting the in-plane motion of the stars. The horizontal phase mixing might have triggered the mixture of Gulliver 21, the intermediate group, and the Collinder 132 moving group, resulting in the formation of the stream.

6. Summary

In this study we have used Gaia DR 3 data to study the Collinder 132–Gulliver 21 region, with the motivation to identify the relationship between the 275 Myr old Gulliver 21 and the 25 Myr old Collinder 132 moving group. Eight subgroups of stars are identified in the target region using StarGO. Our results can be summarized as follows:

1. Eight subgroups in the region of Collinder 132 and Gulliver 21 are divided into three comoving populations: (i) the youngest 25 Myr old Collinder 132 moving group (ASCC 32, Collinder 132 gp 1–4); (ii) an intermediate-

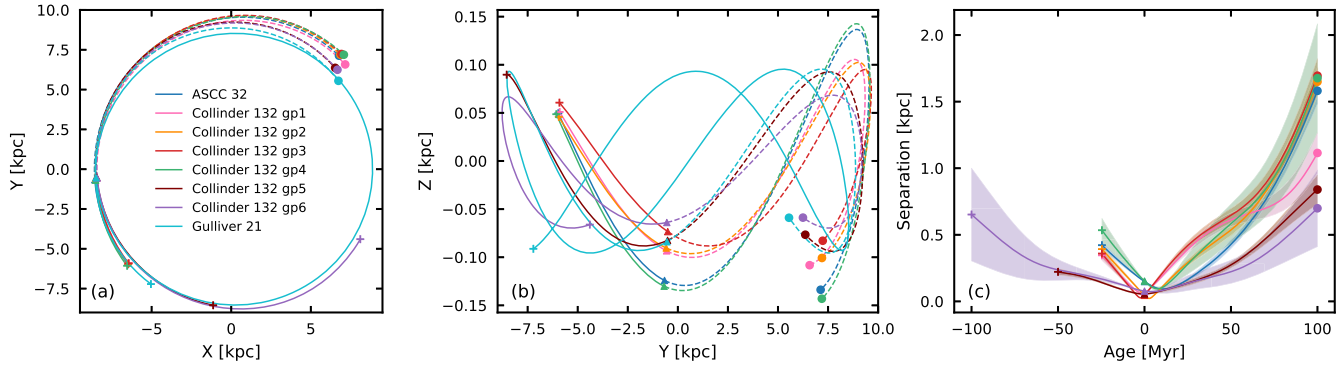

Figure 6. (a–b) Past and future 100 Myr integrated orbits of the eight subgroups in the Collinder 132–Gulliver 21 stream using `Galpy`. (c) Evolution of the separation between seven subgroups and the oldest population, Gulliver 21. The $\pm 1\sigma$ uncertainty interval computed from observational errors in the PM and RV is indicated with the shaded areas. An age of 0 Myr corresponds to the present day. The colored plus signs in the three panels indicate the positions of the corresponding subgroups at the time of birth. The triangles represent the present-day positions, and the filled circles indicate the predicated positions at 100 Myr from the present.

age group, consisting of Collinder 132 gp 5–6 (50–100 Myr); and (iii) the oldest population, Gulliver 21 (275 Myr).

2. In the U–V velocity distribution, three populations stand out as parallel diagonal stripes, following a tight U–V correlation (with identical slope) with a V difference of 30 km s^{-1}. The elongated overdensity generated by these three populations in the U–V space is unique, compared to clusters or groups in the solar neighborhood. It resembles the kinematic structures of moving groups and indicates a comoving state for each population. We name the kinematic structure formed by these three moving groups the Collinder 132–Gulliver 21 stream.
3. The 3D spatial distribution of the Collinder 132–Gulliver 21 stream extends 270 pc. The oldest population, Gulliver 21, is spatially surrounded by the Collinder 132 moving group and the intermediate-age group. All three comoving populations are gravitationally unbound and are undergoing disruption.
4. The Collinder 132–Gulliver 21 stream has a dynamical origin. The young Collinder 132 moving group was born in the spiral arm from filamentary star formation in its natal GMC. The Galactic bar and spiral structure resonance may then have scattered Gulliver 21 and the intermediate-age group toward the location of the Collinder 132 moving group. Three populations began to comove as their orbits overlapped. After 50 Myr from the present time, three comoving populations in the Collinder 132–Gulliver 21 stream will start to separate. The stream will eventually disappear. Stars in each population will continue to comove for (at least) another 100 Myr and will subsequently become three separate moving groups.

The orbit integration carried out in this work is based on axisymmetric Galactic potential. A time-varying potential with perturbation is worth investigating in the future. Although there are indications of abundance variation of 0.3 dex between the youngest Collinder 132 moving group and the oldest population Gulliver 21, high-resolution spectroscopy is required to verify the inhomogeneous metallicity in the Collinder 132–Gulliver 21 stream.

We thank the anonymous referee for their constructive comments and suggestions that helped to improve this paper. This work is supported by the grant of the National Natural Science Foundation of China, No. 12173029. X.P. acknowledges the financial support of the research development fund of Xi'an Jiaotong-Liverpool University (RDF-18–02–32). L.W. thanks the support from the one-hundred-talent project of Sun Yat-sen University, the Fundamental Research Funds for the Central Universities, Sun Yat-sen University (22hytd09), and the National Natural Science Foundation of China through grant 12073090. X.P. and L.W. acknowledge the research support from the National Natural Science Foundation of China through grants 12233013. M.B.N.K. acknowledges support from the National Natural Science Foundation of China (grant 11573004) and Xi'an Jiaotong-Liverpool University (grant RDF-SP-93). Z.Y.L. is supported by the National Natural Science Foundation of China under grant No. 12122301, by a Shanghai Natural Science Research grant (21ZR1430600), by the Cultivation Project for LAMOST Scientific Payoff and Research Achievement of CAMS-CAS, and by the "111" project of the Ministry of Education under grant No. B20019.

This work made use of data from the European Space Agency (ESA) mission Gaia (https://www.cosmos.esa.int/gaia), processed by the Gaia Data Processing and Analysis Consortium (DPAC, https://www.cosmos.esa.int/web/gaia/dpac/consortium). This study also made use of the SIMBAD database and the VizieR catalog access tool, both operated at CDS, Strasbourg, France.

Software: `Astropy` (Astropy Collaboration et al. 2013, 2018), `SciPy` (Millman & Aivazis 2011), `TOPCAT` (Taylor 2005), and StarGO (Yuan et al. 2018).

Appendix A
Member Selection with StarGO

The StarGO (STARs Galactic Origin; Yuan et al. 2018) software, based on the Self-Organizing Map (SOM) algorithm, is able to map high-dimensional data onto a 2D neural network and to search for groupings in the multidimensional parameter space. The SOM algorithm works as follows: First, a 2D neural network is generated with either 100×100 or 150×150 neurons, depending on the number of input stars. Second, each neuron is given a random vector that matches the dimension of the input data, i.e., a 5D weight vector that matches with the 5D input data set, X, Y, Z, $\mu_\alpha \cos\delta$, and μ_δ, is generated. Third, we train a 2D neural network by feeding the input data (stars) one by one to the 2D neural network. StarGO will identify the neuron whose 5D weight vector is closest to the input data. This identified neuron and its neighboring neurons will have

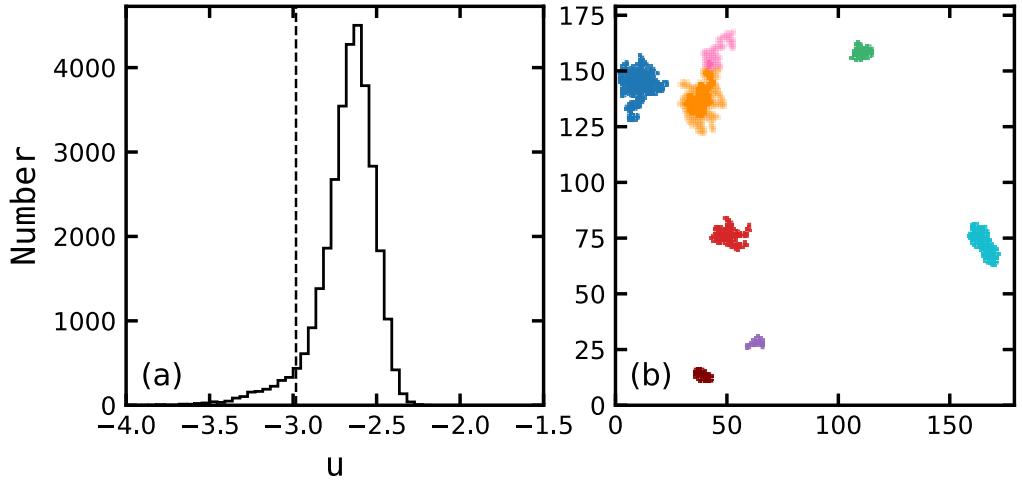

Figure A1. (a) Histogram of the distribution of u-matrix elements. The vertical dashed line denotes the threshold value of u that gives a 10% contamination rate for the identified groups, corresponding to the color patches in the 2D neural network (panel (b)). (b) Neural network generated by SOM. Neurons with a u-threshold corresponding to a 10% contamination rate are shown as colored patches. The transparent pink and orange patches are considered as the top-level structure overall. Solid pink and orange patches are the cores of the secondary hierarchical structures, which correspond to Collinder 132 gp 1 (pink) and group 2 (orange). Other red, green, maroon, purple, and cyan patches correspond to Collinder 132 gp 3, Collinder 132 gp 4, Collinder 132 gp 5, Collinder 132 gp 6, and Gulliver 21 with a contamination rate of 10%, respectively.

their 5D weight vector updated to be closer to the associated input data. Each training iteration of the 2D neural network is finished after looping every star in the target sky region. After each training iteration, the 2D neural network will have patches of neurons sharing similar 5D weight vectors. This training cycle is set to iterate 400 times for convergence.

The difference between the weight vectors of adjacent neurons on the 2D neural network is defended as the u-value. Therefore, the smaller the u-values, the higher the likelihood of stars associated with the neuron to be located in the same stellar group. Each input datum (stars) is associated with the neuron that has a minimum difference in the 5D weight vector. Figure A1(a) shows the histogram of the u-value from the 2D neural network of the Collinder 132–Gulliver 21 sky region. The vertical dashed line shows the threshold cut, which gives a 10% contamination rate for the identified groups. The field-star contamination rate is estimated using the mock Gaia EDR 3 catalog (Rybizki et al. 2020). We process the field stars in the mock Gaia EDR 3 catalog via the same procedure mentioned in the previous paragraph. Those mock stars attached to the patches of members in the 2D neural network trained by the observational data are considered as false positives, i.e., field-star contaminants. Figure A1(b) show patches of neurons corresponding to a 10% contamination rate.

Appendix B
Member List

Table B1 provides a detailed member list of the Collinder 132–Gulliver 21 stream determined by this study.

ORCID iDs

Xiaoying Pang https://orcid.org/0000-0003-3389-2263
Shih-Yun Tang https://orcid.org/0000-0003-4247-1401
Long Wang https://orcid.org/0000-0001-8713-0366
Yanshu Wang https://orcid.org/0000-0002-1243-8224
Zhao-Yu Li https://orcid.org/0000-0001-5017-7021
M. B. N. Kouwenhoven https://orcid.org/0000-0002-1805-0570
Mario Pasquato https://orcid.org/0000-0003-3784-5245

References

Andrae, R., Fouesneau, M., Sordo, R., et al. 2022, A&A, arXiv:2206.06138
Antoja, T., Figueras, F., Fernández, D., & Torra, J. 2008, A&A, 490, 135
Antoja, T., Helmi, A., Bienayme, O., et al. 2012, MNRAS: Letters, 426, L1
Antoja, T., Helmi, A., Romero-Gomez, M., et al. 2018, Natur, 561, 360
Astropy Collaboration, Price-Whelan, A. M., Sipőcz, B. M., et al. 2018, AJ, 156, 123
Astropy Collaboration, Robitaille, T. P., Tollerud, E. J., et al. 2013, A&A, 558, A33
Bania, T. M., Anderson, L. D., & Balser, D. S. 2012, ApJ, 759, 96
Barros, D. A., Pérez-Villegas, A., Lépine, J. R. D., Michtchenko, T. A., & Vieira, R. S. S. 2020, ApJ, 888, 75
Baumgardt, H., & Kroupa, P. 2007, MNRAS, 380, 1589
Beccari, G., Boffin, H. M. J., & Jerabkova, T. 2020, MNRAS, 491, 2205
Bensby, T., Feltzing, S., & Oey, M. S. 2014, A&A, 562, A71
Bensby, T., Oey, M. S., Feltzing, S., & Gustafsson, B. 2007, ApJ, 655, L89
Boffin, H. M. J., Jerabkova, T., Beccari, G., & Wang, L. 2022, MNRAS, 514, 3579
Bovy, J. 2015, ApJS, 216, 29
Bovy, J., & Hogg, D. W. 2010, ApJ, 717, 617
Bressan, A., Marigo, P., Girardi, L., et al. 2012, MNRAS, 427, 127
Cantat-Gaudin, T., Anders, F., Castro-Ginard, A., et al. 2020, A&A, 640, A1
Cantat-Gaudin, T., Jordi, C., Vallenari, A., et al. 2018, A&A, 618, A93
Carrera, R., Pasquato, M., Vallenari, A., et al. 2019, A&A, 627, A119
Chen, B. Q., Li, G. X., Yuan, H. B., et al. 2020, MNRAS, 493, 351
Chen, Y., Bressan, A., Girardi, L., et al. 2015, MNRAS, 452, 1068
Churchwell, E., Povich, M. S., Allen, D., et al. 2006, ApJ, 649, 759
Churchwell, E., Watson, D. F., Povich, M. S., et al. 2007, ApJ, 670, 428
Clariá, J. J. 1977, PASP, 89, 803
Collinder, P. 1931, AnLun, 2, B1
Cottaar, M., Meyer, M. R., & Parker, R. J. 2012, A&A, 547, A35
Creevey, O. L., Sordo, R., Pailler, F., et al. 2022, arXiv:2206.05864
Dame, T. M., Hartmann, D., & Thaddeus, P. 2001, ApJ, 547, 792
De Simone, S., Wu, R. X., & Tremaine, S. 2004, MNRAS, 350, 627
Dehnen, W. 2000, AJ, 119, 800
Eggen, O. J. 1983, AJ, 88, 197
Eggen, O. J. 1996, AJ, 112, 1595
Fleck, J. J., Boily, C. M., Lançon, A., & Deiters, S. 2006, MNRAS, 369, 1392
Gagné, J., Faherty, J. K., Moranta, L., & Popinchalk, M. 2021, ApJL, 915, L29
Gaia Collaboration, Brown, A. G. A., Vallenari, A., et al. 2018a, A&A, 616, A1
Gaia Collaboration, Brown, A. G. A., Vallenari, A., et al. 2021, A&A, 649, A1
Gaia Collaboration, Katz, D., Antoja, T., et al. 2018b, A&A, 616, A11
Gaia Collaboration, Vallenari, A., Brown, A., et al. 2022, A&A, in press, doi:10.1051/0004-6361/202243940
Green, G. M., Schlafly, E., Zucker, C., Speagle, J. S., & Finkbeiner, D. 2019, ApJ, 887, 93

He, Z., Wang, K., Luo, Y., et al. 2022, arXiv:2206.12170
Hou, L. G., & Gao, X. Y. 2014, MNRAS, 438, 426
Jerabkova, T., Boffin, H. M. J., Beccari, G., & Anderson, R. I. 2019, MNRAS, 489, 4418
Katz, D., Sartoretti, P., Guerrier, A., et al. 2022, arXiv:2206.05902
Kounkel, M., & Covey, K. 2019, AJ, 158, 122
Kushniruk, I., Bensby, T., Feltzing, S., et al. 2020, A&A, 638, A154
Kushniruk, I., Schirmer, T., & Bensby, T. 2017, A&A, 608, A73
Lee, J., Song, I., & Murphy, S. J. 2022, MNRAS, 511, 6179
Li, H., & Widrow, L. M. 2021, MNRAS, 503, 1586
Li, Y., Pang, X., & Tang, S.-Y. 2021, RNAAS, 5, 173
Li, Z.-Y. 2021, ApJ, 911, 107
Li, Z.-Y., & Shen, J. 2020, ApJ, 890, 85
Liu, L., & Pang, X. 2019, ApJS, 245, 32
McMillan, S. L. W., Vesperini, E., & Portegies Zwart, S. F. 2007, ApJL, 655, L45
Messina, S., Nardiello, D., Desidera, S., et al. 2022, A&A, 657, L3
Millman, K. J., & Aivazis, M. 2011, CSE, 13, 9
Minchev, I., Boily, C., Siebert, A., & Bienayme, O. 2010, MNRAS, 407, 2122
Miret-Roig, N., Galli, P. A. B., Brandner, W., et al. 2020, A&A, 642, A179
Miville-Deschênes, M.-A., & Lagache, G. 2005, ApJS, 157, 302
Pang, X., Grebel, E. K., Allison, R. J., et al. 2013, ApJ, 764, 73
Pang, X., Li, Y., Tang, S.-Y., Pasquato, M., & Kouwenhoven, M. B. N. 2020, ApJL, 900, L4
Pang, X., Li, Y., Yu, Z., et al. 2021a, ApJ, 912, 162
Pang, X., Tang, S.-Y., Li, Y., et al. 2022, ApJ, 931, 156
Pang, X., Yu, Z., Tang, S.-Y., et al. 2021b, ApJ, 923, 20
Pinfield, D. J., Jameson, R. F., & Hodgkin, S. T. 1998, MNRAS, 299, 955
Recio-Blanco, A., de Laverny, P., Palicio, P. A., et al. 2022, arXiv:2206.05541
Reid, M. J., Menten, K. M., Brunthaler, A., et al. 2019, ApJ, 885, 131
Riello, M., De Angeli, F., Evans, D. W., et al. 2021, A&A, 649, A3
Rybizki, J., Demleitner, M., Bailer-Jones, C., et al. 2020, PASP, 132, 074501
Sellwood, J. A., & Binney, J. J. 2002, MNRAS, 336, 785
Simpson, R. J., Povich, M. S., Kendrew, S., et al. 2012, MNRAS, 424, 2442
Skuljan, J., Hearnshaw, J. B., & Cottrell, P. L. 1999, MNRAS, 308, 731
Tang, S.-Y., Pang, X., Yuan, Z., et al. 2019, ApJ, 877, 12
Taylor, M. B. 2005, in ASP Conf. Ser. 347, Astronomical Data Analysis Software and Systems XIV, ed. P. Shopbell, M. Britton, & R. Ebert (San Francisco, CA: ASP), 29
Wang, L., & Jerabkova, T. 2021, A&A, 655, A71
Yan, Q.-z., Xu, Y., Zhang, B., et al. 2016, AJ, 152, 117
Yuan, Z., Chang, J., Banerjee, P., et al. 2018, ApJ, 863, 26
Yuan, Z., Chang, J., Beers, T. C., & Huang, Y. 2020a, ApJL, 898, L37
Yuan, Z., Myeong, G. C., Beers, T. C., et al. 2020b, ApJ, 891, 39
Zhang, J., Zhao, J., Oswalt, T. D., et al. 2019, ApJ, 887, 84
Zhao, J., Zhao, G., & Chen, Y. 2009, ApJL, 692, L113